Multifrequency ESEEM Spectroscopy of Sulfite Oxidase in Phosphate Buffer: Direct Evidence for Coordinated Phosphate

Andrew Pacheco, Partha Basu, Petr Borbat, Arnold M. Raitsimring,* and John H. Enemark*

Department of Chemistry, University of Arizona, Tucson, Arizona 85721

Received June 28, 1996[⊗]

The molybdenum(V) coordination environment of sulfite oxidase has been investigated by multifrequency ESEEM spectroscopy in ∼70 mM phosphate buffer at pH* = 6.5 in both H_2O and D_2O. The FT-ESEEM spectra in H_2O typically consist of three lines. One of these lines is always close to twice the Larmor frequency of the P atom ($2\nu_P$) and is assigned to one or more coordinated phosphates, providing the first direct unambiguous detection of such coordination. Extensive simulations of this phosphate signal at the various operational frequencies indicated that the coordinated phosphate group(s) probably does (do) not adopt a fixed orientation, and as a result, a description of the Mo···P hyperfine interaction required the introduction of a distribution of such orientations, with Mo···P distance(s) of 3.2−3.3 Å. The other two lines in the FT-ESEEM spectra in H_2O, located at ν_H and $2\nu_H$, were assigned to matrix protons. In D_2O buffer two additional lines, assigned to matrix deuterons, were also seen.

Introduction

Sulfite oxidase (SO) is an essential enzyme for sulfur metabolism in animals,[1] catalyzing the oxidation of sulfite to sulfate, with the concomitant reduction of 2 equiv of ferricytochrome *c*:

$$SO_3^{2-} + 2(\text{cyt}c^{III}) + H_2O \rightarrow SO_4^{2-} + 2(\text{cyt}c^{II}) + 2H^+$$

More generally, SO is one member of a diverse group of enzymes, all of which contain a mononuclear Mo center and catalyze 2-electron oxidations or reductions by what is effectively an oxo-transfer process:[2−5]

$$X + H_2O \rightleftharpoons XO + 2H^+ + 2e^-$$

A key distinguishing structural characteristic of these enzymes is that the Mo atoms are coordinated by the dithiolene side chain of one or two novel 6-substituted pterin ligands (structure **1**).[5,6]

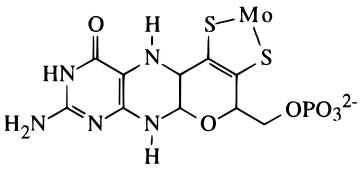

1

In his recent review, Hille[5] divides this group of molybdenum-containing enzymes into three subclasses, based on their reactivity and spectroscopic characteristics. The enzymes in the first and largest subclass catalyze the oxidative hydroxylation of a diverse series of aldehydes and heterocycles. Enzymes in the second and third subclasses catalyze oxygen atom transfers between the Mo and an available electron lone pair on the substrate. These latter two subclasses are distinguished from each other by whether or not their electronic spectra exhibit a long-wavelength charge-transfer band. Certain bacterial enzymes, exemplified by DMSO reductase, exhibit such a band, while others such as SO do not.

Recently the crystal structure determinations of aldehyde oxidoreductase (AOR) from *Desulfovibrio gigas* (a representative of the first subclass, which exhibits one pterin per Mo atom),[7] and DMSO reductase from *Rhodobacter sphaeroides* (second subclass, with two pterins per Mo atom)[8] have been reported. The structure of AOR from the hyperthermophilic bacterium *Pyrococcus furiosus*, which has two pterins coordinated to a tungsten atom, has also been reported.[9] To date however, there has been no crystal structure characterization for an enzyme of the subclass to which SO belongs. Consequently, current characterization of these enzymes relies on chemical and spectroscopic investigations.

CW-EPR spectroscopy has proven to be a useful tool for characterizing the Mo(V) state of SO.[2] Three spectroscopically distinct forms of SO have been identified by CW-EPR; one form is obtained pure only in high-pH buffers (9−9.5) containing low concentrations of chloride or phosphate, while the other two are observed at low pH (6.5−7).[10−13] Which of the low-pH forms of the enzyme is observed depends on whether phosphate is present in the buffer.[10] There is also evidence for a species containing a coordinated sulfite, which has an EPR spectrum similar to that of the enzyme in phosphate buffer.[14] In the absence of phosphate, CW-EPR spectra of SO at low[10,12]

* Authors to whom correspondence should be addressed.
[⊗] Abstract published in *Advance ACS Abstracts*, November 1, 1996.

(1) Rajagopalan, K. V. *Nutr. Rev.* **1987**, *45*, 321−328.
(2) *Molybdenum Enzymes*; Spiro, T. G., Ed.; John Wiley and Sons: New York, 1985.
(3) *Molybdenum and Molybdenum-Containing Enzymes*; Coughlan, M. P., Ed.; Pergamon Press: Oxford, U.K., 1980.
(4) (a) Enemark, J. H.; Young, C. G. *Adv. Inorg. Chem.* **1993**, *40*, 1. (b) Pilato, R. S.; Stiefel, E. I. In *Inorganic Catalysis*; Reedijk, J., Ed.; Marcel Dekker, Inc.: New York, 1993; p 131.
(5) Hille, R. *Chem. Rev.* **1996**, *96*, 2757−2816.
(6) Rajagopalan, K. V. *Adv. Enzymol. Relat. Areas Mol. Biol.* **1991**, *64*, 215.
(7) Romao, M. J.; Archer, M.; Moura, I.; Moura, J. J. G.; LeGall, J.; Engh, R.; Schneider, M.; Hof, P.; Huber, R. *Science* **1995**, *270*, 1170−1176.
(8) Schindelin, H.; Kisker, C.; Hilton, J.; Rajagopalan, K. V.; Rees, D. C. *Science* **1996**, *272*, 1615−1621.
(9) Chan, M. K.; Mukund, S.; Kletzin, A.; Adams, M. W. W.; Rees, D. C. *Science* **1995**, *267*, 1463−1465.
(10) Lamy, M. T.; Gutteridge, S.; Bray, R. C. *Biochem. J.* **1980**, *185*, 397−403.
(11) Gutteridge, S.; Lamy, M. T.; Bray, R. C. *Biochem. J.* **1980**, *191*, 285−288.
(12) Bray, R. C.; Gutteridge, S.; Lamy, M. T.; Wilkinson, T. *Biochem. J.* **1983**, *211*, 227−236.
(13) Bray, R. C. *Polyhedron* **1986**, *5*, 591−595.

S0020-1669(96)00780-X CCC: $12.00

Scheme 1

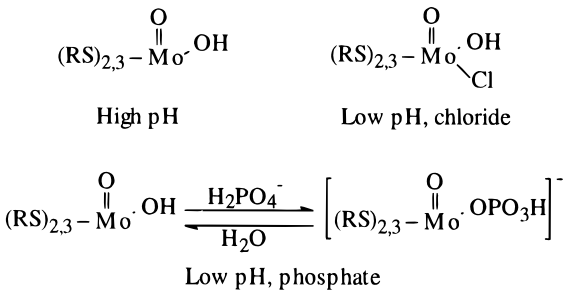

and high[15] pH clearly show hyperfine interaction of the electron with a single strongly coupled exchangeable proton, which has been assigned to a Mo−OH group. This interaction is not observed in phosphate buffer, which implies that under these conditions a phosphate group coordinates to the Mo center, displacing the OH group.[11] Combining the CW-EPR data with EXAFS studies at the Mo K edge on oxidized and reduced SO has led to the structural proposals of Scheme 1 for the Mo(V) states of SO.[16]

In principle, any atoms near the Mo with nonzero nuclear spin ($I > 0$) can give rise to hyperfine interactions, yielding direct information about what ligands may be coordinated to the metal center. However, such hyperfine splittings are often quite small for oxo−Mo(V) centers, which typically adopt approximate tetragonal geometry; the $4d^1$ electron configuration of these centers places the unpaired electron in an essentially nonbonding orbital, which points between the donor atoms of the ligands. Attempts to detect small splittings in SO spectra by standard CW-EPR have necessitated pushing the technique to its limits. Nevertheless, Bray *et al*. obtained evidence for direct coordination of phosphate to the Mo center of SO in phosphate buffer from careful difference measurements between ^{17}O-labeled and ordinary phosphate.[11] In a later paper George *et al*. proposed, on the basis of an analysis of the third-derivative spectrum of the phosphate form of SO, that this form of the enzyme actually has two inequivalently coupled phosphates coordinated to the Mo center.[17]

Unlike conventional CW-EPR, electron−nuclear double resonance (ENDOR) spectroscopy, and electron spin-echo envelope modulation (ESEEM) spectroscopy are powerful techniques ideally suited for detecting weak hyperfine and quadrupole interactions. To date there has been only one ENDOR[18] and no ESEEM studies of SO, despite the abundance of data from conventional CW-EPR spectroscopy available for this and related enzymes. Our interest in the coordination environment of Mo in SO has prompted us to carry out such studies in a variety of buffers to further structurally characterize the various forms of the enzyme. Here we present multifrequency ESEEM results for SO in phosphate buffer at pH 6.5, which have allowed us to directly detect the presence of phosphate(s) coordinated to the Mo(V) center.

Materials and Methods

High-purity SO for the EPR and ESE experiments was obtained from chicken livers using a procedure similar to that of Sullivan *et al*.[19] and showed a A_{414}/A_{280} ratio of 0.84 in its UV/visible spectrum. Fully oxidized SO stock was pre-equilibrated with a phosphate buffer of ionic strength $\mu = 0.15$ and pH* = 6.5, made up in either H_2O or D_2O, using a Centricon concentrator (Amicon). To the equilibrated SO solution (~60 μL) was added 10 μL of 0.11 M sulfite stock solution, made up in the same phosphate buffer. The resulting reduced enzyme was then immediately frozen in liquid nitrogen. The final SO concentration for the experiments was ~0.6 mM.

Continuous-wave EPR spectra were obtained at 77 K on a Bruker ESP-300E spectrometer operating at X-band. Microwave frequencies were measured with a Systron Donner counter. Pulsed EPR studies were performed on a home-built broad-band spectrometer operating at 8−18 GHz.[20] Measurements were made at 7 microwave frequencies (ν_0) within the 8.9−15.3 GHz range in steps of ~1 GHz; the available cryostat precluded investigation of frequencies above 15.4 GHz (*vide infra*).

The fast relaxation of the Mo center required that ESEEM measurements be performed far below 77 K. This was achieved by building a set of reflecting cavities that mate to an available Oxford ESR 900 continuous-flow cryostat. Modification of the insert tube of the cryostat allows ν_0 to be as high as 15.26−15.4 GHz. All measurements were performed at 20 K. This temperature yielded the optimal acquistion time at a given signal/noise ratio and allowed a repetition rate of 400 Hz without signal saturation. In primary echo experiments, two microwave pulses of equal amplitude and duration were used to generate an echo signal. The duration of the pulses was varied from 26 to 15 ns in order to maintain approximately similar orientational selection and excitation conditions as ν_0 was varied. The nominal angle of the resonant spin rotation was $2\pi/3$. In three pulse experiments, three $\pi/2$ pulses of the same duration were used. The interval between pulses varied from 300 (the dead time for these types of cavities) to 2300 ns. For frequencies of <13 GHz the interval was incremented in 10 ns steps; for frequencies of >13 GHz steps of 5 ns were used. The number of accumulations at each step depended upon the signal amplitude, which in turn depended on the field position of data collection, and was about 1000−4000 for a boxcar gate width of 15 ns. Such measurements were performed across the entire EPR spectrum in steps of 5 G. ESEEM spectra were obtained by Fourier transformation of the experimental time domain data. Before the FT procedure an exponential fit was used to normalize the decaying time domain data to unity, and a low low-order polynomial fit was used to subtract the nonmodulated part of the spin-echo signal. For a given set of experimental conditions, the nominal accuracy of the measurements of the spectral peak position in an FT ESEEM spectrum was ±0.03 MHz. However, in some measurements the spectral lines did not have well-determined maxima, which increased the uncertainty in peak position. The normalized noise level (for unity signal) in an FT spectrum depends upon the operational frequency. At 8.9 MHz the sensitivity was better than 2.5×10^{-3} and improved to 1.0×10^{-3} as the operational frequency increased to 15.4 MHz.

Results

The CW-EPR spectrum of the phosphate form of sulfite oxidase in frozen D_2O is shown in Figure 1. The resolved rhombic spectrum exhibits principal g values of 1.965, 1.973, and 1.995. The individual line widths are estimated to be ~3 G. The same spectrum, but with slightly larger individual line widths (~5 G), was observed for a similar sample prepared in H_2O.

Two representative examples of ESEEM time domain data at low and high ν_0's are shown in Figure 2. As one can see from Figure 2, the characteristic decay rate is ~0.6 μs^{-1} and

(14) Bray, R. C.; Lamy, M. T.; Gutteridge, S.; Wilkinson, T. *Biochem. J.* **1982**, *201*, 241−243.
(15) In the high-pH case, the hyperfine interaction is not observed under normal conditions; however, at high microwave powers, two satellite signals appear to either side of the low-field EPR signal, which are attributable to simultaneous transitions of electron and nuclear spins: George, G. N. *J. Magn. Reson.* **1985**, *64*, 384−394.
(16) George, G. N.; Kipke, C. A.; Prince, R. C.; Sunde, R. A.; Enemark, J. H.; Cramer, S. P. *Biochemistry* **1989**, *28*, 5075−5080.
(17) George, G. N.; Prince, R. C.; Kipke, C. A.; Sunde, R. A.; Enemark, J. H. *Biochem. J.* **1988**, *256*, 307−309.
(18) Howes, B. D.; Bennet, B.; Koppenhofer, A.; Lowe, D. J.; Bray, R. C. *Biochemistry* **1991**, *30*, 3969−3975.
(19) Sullivan, E. P.; Hazzard, J. T.; Tollin, G.; Enemark, J. H. *Biochemistry* **1993**, *32*, 12465−12470.
(20) Borbat, P.; Raitsimring, A. New Pulse EPR Spectrometer at the University of Arizona In *Abstracts of 36th Rocky Mountain Conference on Analytical Chemistry*, Denver, CO, July 31−August 5, 1994; p 94.

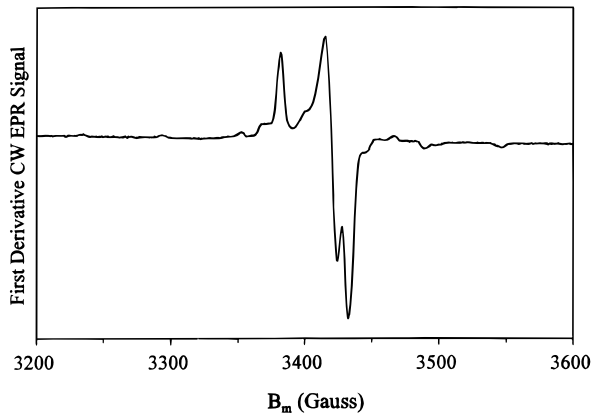

Figure 1. First-derivative CW-EPR spectrum of the Mo(V) center of SO in deuterated phosphate buffer: pH* = 6.5. $T = 77$ K; $\nu_0 = 9.4401$ GHz; power, 0.2 mW; modulation amplitude, 2.85 G; modulation frequency, 100 kHz.

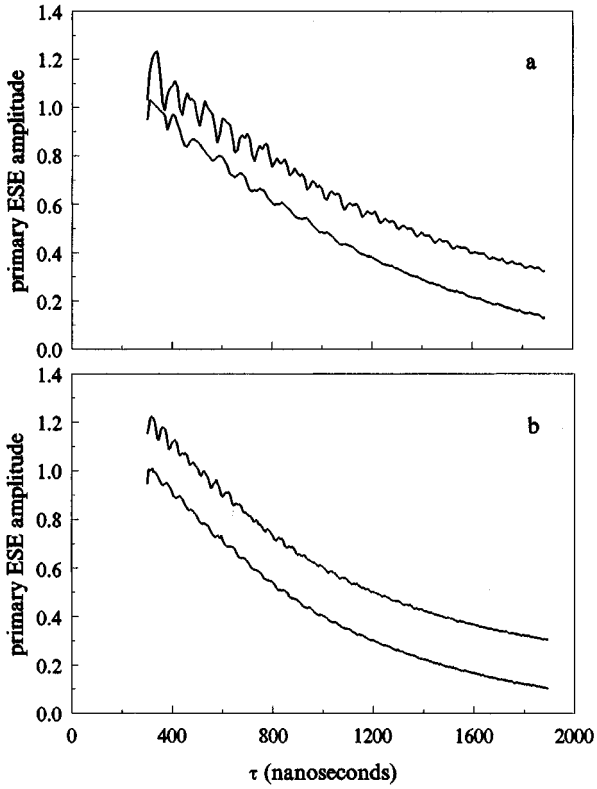

Figure 2. Primary ESEEM of an SO sample, analogous to that described in Figure 1 but made up in H_2O, collected at two operational (ν_0) frequencies. Top curves, initial experimental data; bottom curves, the same data after rejection filtration of H-related modulation. Acquisition conditions: $T = 20$ K; repetition rate, 400 Hz; dead time, 300 ns; nominal flib angle, $2\pi/3$. (a) $\nu_0 = 15.281$ GHz; $B_m = 5526$ G; pulse duration, 15 ns; step, 5 ns. (b) $\nu_0 = 8.904$ GHz; $B_m = 3238$ G; pulse duration, 26 ns; step, 10 ns.

does not vary substantially with ν_0. Judging from results obtained for a series of mononuclear Mo(V) model complexes, this relaxation rate is unusually high for a Mo(V) center. Additional investigations showed that neither instantaneous diffusion nor spectral diffusion due to electron−nuclear interaction are the cause of this rapid relaxation; another possibility would be spectral diffusion caused by interaction of the Mo centers with residual paramagnetic iron centers, which are an intrinsic component of the oxidized form of the enzyme. Representative FT-ESEEM spectra (primary echo) are shown in Figure 3. The spectra in H_2O (Figure 3a,b) consist of three lines. One of these lines is close to twice the Larmor frequency

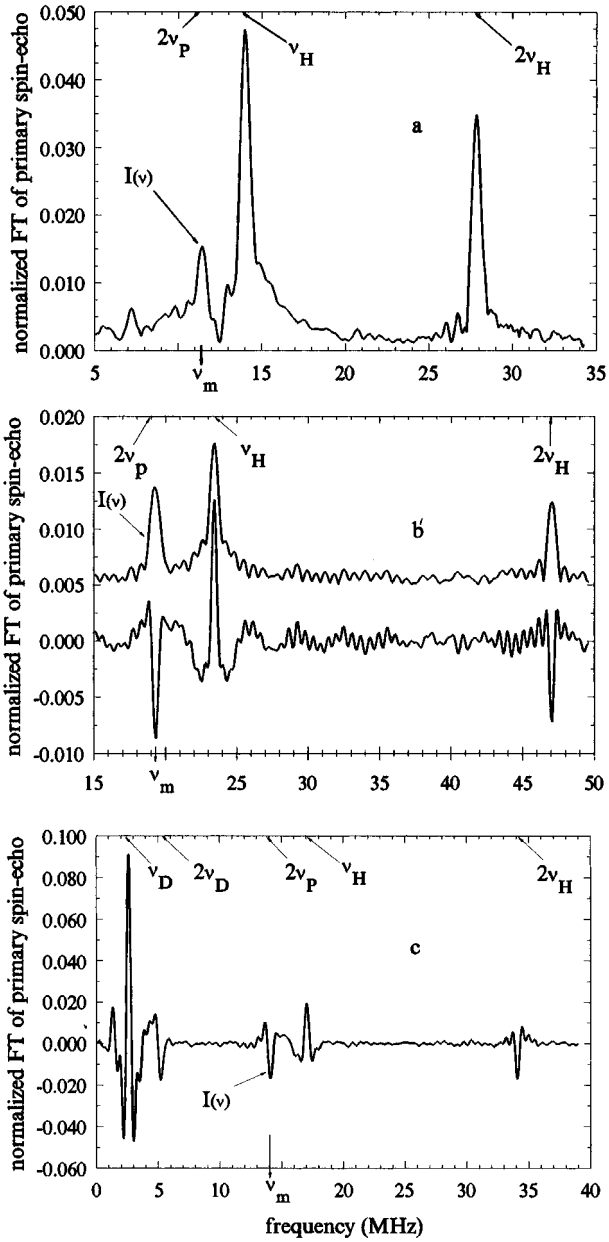

Figure 3. Normalized ESEEM spectra of SO in protonated and deuterated phosphate buffers, at various operational frequencies. Spectra a and b result from FT of the data presented in Figure 2 a and b, respectively; spectrum c is of the sample prepared in deuterated buffer, described in Figure 1: (a) magnitude FT; (b) magnitude FT (top), cosine FT (bottom); (c) cosine FT of time domain data collected at $\nu_0 = 11.001$ GHz, $B_m = 4000$ G; pulse duration, 22 ns; step, 10 ns. The spectral lines related to Mo(V)···P interaction are denoted as $I(\nu)$. The frequency at which this line reaches a maximum amplitude is indicated by ν_m at the bottom of the frame. Arrows at the top of the frame mark the positions of the nuclear Larmor frequencies and double nuclear Larmor frequencies of D, H, and P at the given fields.

of the P atom ($2\nu_P$), and will henceforth be referred to as $I(\nu)$. Two other lines due to protons are located at ν_H and $2\nu_H$. For the sample prepared in D_2O buffer two additional lines are seen, at the deuteron Larmor frequency (ν_D), and at twice this frequency ($2\nu_D$) (Figure 3c). The normalized amplitude of $I(\nu)$ at a fixed ν_0 depends on field position (g value), and varies by a factor of 2−4 as the field is swept. An example of such dependence is shown in Figure 4. At each field position $I(\nu)$ reaches a maximum, $I(\nu_m)$, at a certain frequency ν_m. From the set of $I(\nu_m)$ one can choose the maximal one, $I^*(\nu_m)$ and corresponding frequency ν^*_m. The frequency ν^*_m, and the maximum amplitude value itself, $I^*(\nu_m)$, depend on ν_0. Figure

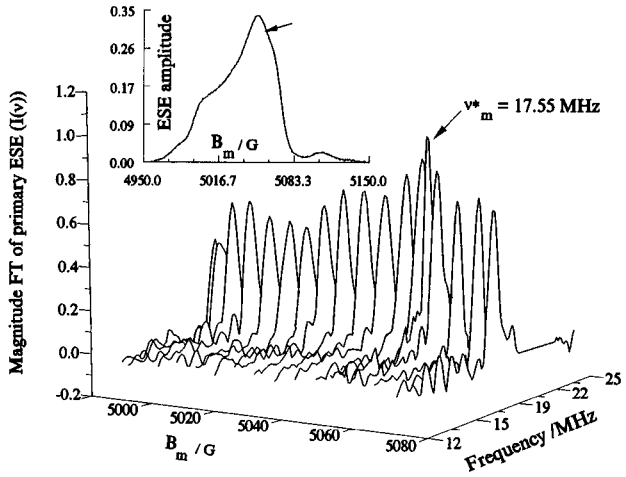

Figure 4. Example of the $I(\nu)$ (magnitude FT) peak position and intensity varying as the magnetic field is swept at a constant operational frequency ($\nu_0 = 13.943$ GHz). The sample used was that described in Figure 2. Proton-related lines are zeroed to avoid overlapping. The unit of modulation amplitude (Z axis) is 0.012. Inset: ESE-detected spectrum at the given operational frequency; the arrow marks the magnetic field where $I(\nu)$ reaches the maximal amplitude, $I^*(\nu_m)$. The arrow in the main figure marks ν^*_m.

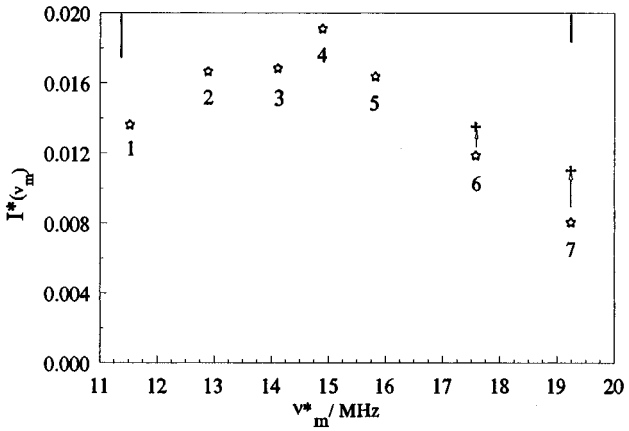

Figure 5. Stars: experimentally observed dependence of $I^*(\nu_m)$ on ν^*_m at various operational frequencies. Values for ν_0, B_m, and g, respectively: (1) 8.904 GHz, 3238 G, 1.965; (2) 10.074 GHz, 3667 G, 1.963; (3) 11.001 GHz, 4000 G, 1.965; (4) 11.754 GHz, 4270 G, 1.967; (5) 12.487 GHz, 4540 G, 1.965; (6) 13.943 GHz, 5056 G, 1.970; (7) 15.281 GHz, 5526 G, 1.975. Crosses: $I^*(\nu_m)$ values expected at the highest operational frequencies if full excitation could be achieved. The solid bars at the upper right- and left-hand corners represent the experimental accuracy in modulation amplitude measurements.

5 shows a parametric plot of the maximal modulation amplitude of $I^*(\nu_m)$ vs its frequency, ν^*_m, for seven experimental values of ν_0. These $I^*(\nu_m)$'s vary from $1.3 \pm 0.13\%$ at $\nu_0 = 8.9$ GHz to $0.85 \pm 0.06\%$ at $\nu_0 = 15.26$ GHz and reach a weak maximum of 1.70−1.9% at $\nu_0 = 10-12.7$ GHz. At the highest ν_0 frequencies the condition of full excitation could not be fulfilled, and consequently the modulation amplitude was underevaluated. The loss of modulation amplitude of $I(\nu)$ at high ν_0 was corrected for by using the dependence of the amplitude of the proton line at $2\nu_H$ on ν_0 as an internal standard, in accord with Astashkin *et al.*[21] The corrected amplitudes of $I^*(\nu_m)$s are also shown in Figure 5.

As is well-known from the theory of ESEEM,[22] each spectral line is characterized not only by an amplitude and position but also by a relative sign. In the cosine Fourier-transformed

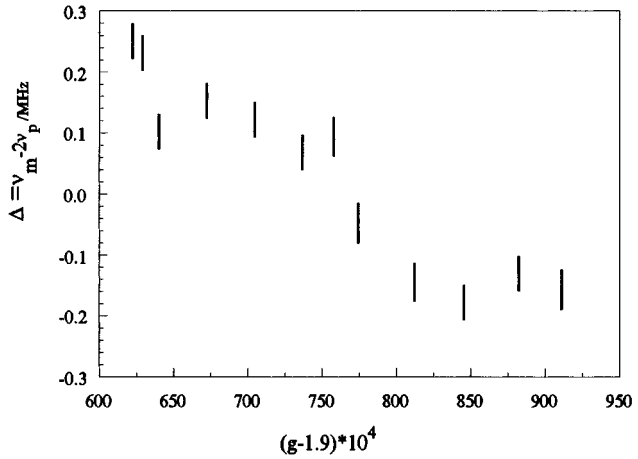

Figure 6. Shifts (Δ) of ν_m from the double Larmor P frequency, at $\nu_0 = 10.074$ GHz, as a function of g value (field position).

spectrum, the signs of the basic harmonics are positive whereas the signs of the combination harmonics are negative. Moreover, for weakly coupled nuclei the basic harmonics appear at the nuclear Larmor frequency (ν_I) and the combination frequencies appear near twice the Larmor frequencies ($2\nu_I$). Thus, the relative sign of H- and D-related lines must be positive at ν_H (ν_d) and negative at $2\nu_H$ ($2\nu_d$) (see Theory and Discussion). Of particular interest in this study was the sign of the P-related line $I(\nu)$, and shift (Δ) of ν_m from twice the nuclear Larmor frequency, $2\nu_P$. The relative signs of ESEEM lines can be obtained from the cosine FT; however, in order to obtain the correct sign, a dead-time phase correction (PC) is required. Although the PC procedure is quite simple in principle, the finite pulse duration leads to uncertainty in the dead time of a pulse. In addition, PC causes side lobes in the FT, which may obscure a line.[22] This problem was encountered for experiments carried out at $\nu_0 < 11$ GHz, where side lobes from a strong H-related line obscured the weak P-related line. Consequently, reliable PC spectra could only be obtained for data with $\nu_0 \geq 11$ GHz, where the H-related line was becoming weaker and much farther shifted from the P line. To overcome the uncertainty caused by finite pulse duration, the H- and D-related lines were used as internal standards, and the dead time was adjusted from the nominal value (within the limits of the pulse duration), until the phases of these references lines were correct. Examples are shown in Figure 3b,c. The signs of the P-related lines appeared to be negative at $\nu_0 > 11$ GHz, and their shifts (Δ) from $2\nu_P$ were positive. At $\nu_0 = 10.07$ GHz we were able to determine Δ for the magnitude FT line only. Both positive and negative shift values were observed, depending upon field position (Figure 6). Lastly, at $\nu_0 = 8.9$ MHz the strong dependence of the modulation amplitude on field position, and the low sensitivity at this frequency, limited the observable Δ to the magnitude FT spectra in the restricted field range between g_x and g_y. These shifts were positive and varied between 0 and 0.2 MHz.

A stimulated echo was also obtained at each ν_0, for at least two or three field positions and 5−10 time intervals between the first and second pulses. For all experiments, FT ESEEM spectra of the stimulated echo show only a line at ν_H for the sample prepared in H_2O buffer and an additional line at ν_D for the sample prepared in D_2O buffer. No lines related to phosphorus modulation were observed. The lines at ν_H, $2\nu_H$, ν_D, and $2\nu_D$, caused by Mo(V) interaction with nonexchangeable

(21) Astashkin, A. V.; Dikanov, S. A.; Kurshev, V. V.; Tsvetkov, Yu. D. *Chem. Phys. Lett.* **1987**, *136*, 335.

(22) Dikanov, S. A.; Tsvetkov, Yu. D. *Electron Spin Echo Envelope Modulation (ESEEM) Spectroscopy*; CRC Press: Boca Raton, FL, 1992; Chapter 1.

protons of the enzyme and matrix protons (or deuterons in D_2O buffer), are not the subject of this paper, which concentrates on interpretation of the behavior of the line related to the Mo(V)···P interaction(s).

The line related to the Mo(V)···P interaction(s) must arise from P nuclei that are in the vicinity of the Mo(V) center. This line cannot be due to the interaction of Mo(V) with matrix P nuclei because the concentration of phosphate in the buffer was too low (0.068 M). Moreover, there is no line centered at ν_P, which is a characteristic of the interaction of an electron spin with distant nuclei. On the basis of the recent crystal structure determinations of other proteins with molybdopterin cofactors,[7,8] the single phosphate group of the molybdenum cofactor is expected to be at least 7 Å away from the Mo atom and would not be detectable at these operational frequencies.[18] We therefore conclude that the observed line $I(\nu)$ is due to Mo(V) hyperfine interaction with directly coordinated phosphate(s), and the following discussion will focus on these interactions and the structural information concerning the Mo(V) center of the phosphate form of SO that can be extracted from these results.

Theory and Discussion

We start the discussion with the well-known expression for two fundamental frequencies, ν_α and ν_β, of a system that contains an electron spin $S = {}^1/_2$ and a nuclear spin $I = {}^1/_2$, and include the Mo(V)···P system as a particular case:[23,24]

$$\nu_{m_s} = |\vec{h}^{\pm}|; \quad \vec{h}^{\pm} = -\nu_I \mathbf{l} + \frac{\mathbf{Dgl}}{g_e} m_s \tag{1}$$

$$\nu_{m_s} = [(m_s A_1 - \nu_I l_1)^2 + (m_s A_2 - \nu_I l_2)^2 + (m_s A_3 - \nu_I l_3)^2]^{1/2}$$

where $m_s = \pm{}^1/_2$ for the α or β state of the electron spin, respectively, $\mathbf{D} = a\mathbf{E} + \mathbf{D}'$ is the tensor of the hyperfine interaction (HFI), represented as a sum of isotropic and anisotropic terms, $\mathbf{E}$ is the unit matrix, $\mathbf{g}$ is the $\mathbf{g}$ tensor, ν_I is the nuclear Larmor frequency at a given magnetic field (B_m), and $\mathbf{l}$ is a unit vector which coincides with the direction of the external magnetic field $\mathbf{B_m}$:

$$l_1 = \sin\theta\cos\phi; \quad l_2 = \sin\theta\sin\phi; \quad l_3 = \cos\theta \tag{2}$$

The particular form of A_i depends on the reference coordinate frame (RCF) used for the calculations. For systems where $\mathbf{g}$-tensor anisotropy exceeds the anisotropy of the HFI, a convenient RCF is that in which the axes coincide with the principal axes of the $\mathbf{g}$ tensor. In this RCF, and accounting for dipolar (in the point−dipole approximation, PDA) and isotropic contributions to the HFI, the other terms of eq 1 are defined as

$$A_i = T[g_i l_i (g_i(3n_i^2 - 1) + a/T) + 3n_i \sum_{k \neq i} g_k^2 l_k n_k]/g_e$$

$$g_e = (\sum (g_i l_i)^2)^{1/2} \tag{3}$$

$$n_1 = \sin\theta_n \cos\phi_n; \quad n_2 = \sin\theta_n \sin\phi_n; \quad n_3 = \cos\theta_n$$

where n_i are the direction cosines of the radius vector $\mathbf{r}$ connecting the electron and nuclear spins in the RCF, a is the isotropic hyperfine coupling constant, g_i are the principal values of the electronic $\mathbf{g}$ tensor with g_e being the effective electronic g value for a given experiment, and $T = -\beta_e\beta_n g_n/\hbar r^3$, where β_e is the Bohr magneton, β_n is the nuclear magneton, and r is the electron−nuclear distance. The modulation of the primary spin-echo signal $V(\tau)$ for this spin system and a particular orientation of electron and nuclear spins is described by expression[22]

$$V(\tau) \propto 1 - \frac{k}{2}\Big[1 - \cos 2\pi\nu_\alpha\tau - \cos 2\pi\nu_\beta\tau + \frac{1}{2}\cos(2\pi\nu_-\tau) + \frac{1}{2}\cos(2\pi\nu_+\tau)\Big] \tag{4}$$

where ν_+ and ν_- are combinational frequencies, $\nu_\pm = \nu_\alpha \pm \nu_\beta$, and k is defined in eqs 6 and 7. This expression immediately shows that the signs of lines at the fundamental and combinational frequencies are positive and negative, respectively. If the system contains i nuclei,

$$V(\tau) = \prod V^{(i)}(\tau) \tag{5'}$$

For $k \ll 1$ this expression may be rewritten as

$$V(\tau) \propto 1 - \sum_{(i)} \frac{k^{(i)}}{2}\Big[1 - \cos 2\pi\nu_\alpha^{(i)}\tau - \cos 2\pi\nu_\beta^{(i)}\tau + \frac{1}{2}\cos(2\pi\nu_-^{(i)}\tau) + \frac{1}{2}\cos(2\pi\nu_+^{(i)}\tau)\Big] \tag{5}$$

As follows from eq 5, the modulation amplitude (or intensity of the FT-ESEEM spectrum) is proportional to the parameter k. This parameter is the product of allowed and forbidden transition probabilities, and in the same approximation as was applied for deriving fundamental frequencies, $k = \sin^2\eta$, where $\cos\eta$ is determined by expression[25]

$$\cos\eta = \frac{\vec{h}^{+}\vec{h}^{-}}{|\vec{h}^{+}||\vec{h}^{-}|} \tag{6}$$

$$\vec{h}^{\pm} = \left[\left(\frac{A_1}{2} \pm \nu_I l_1\right), \left(\frac{A_2}{2} \pm \nu_I l_2\right), \left(\frac{A_3}{2} \pm \nu_I l_3\right)\right]$$

The explicit expression for k as derived from eq 6 is[26]

$$k = (\nu_I^2/\nu_\alpha^2\nu_\beta^2)\{[A_1 l_2 - A_2 l_1]^2 + [A_2 l_3 - A_3 l_2]^2 + [A_1 l_3 - A_3 l_1]^2\} \tag{7}$$

Therefore, the FT-ESEEM spectrum of the primary spin echo for an $S = {}^1/_2$, $I = {}^1/_2$ system is represented by four lines, $I(\nu_{\alpha,\beta,\pm})$. For a cosine FT the lines are positive at fundamental frequencies and negative at the combinational frequencies. In a disordered system a given field B_m does not represent a unique orientation but rather a set of orientations and, consequently, a set of frequencies. Because the amplitude of modulation also depends on orienatation, eq 5 for such a system must be rewritten as

$$\langle\langle V(\tau)\rangle\rangle \propto 1 - (I_0 - \sum_w I(\nu_w)\cos 2\pi\nu_w\tau) \tag{8}$$

where ν_w is ν_α, ν_β, ν_+ or ν_- and $\langle\langle ... \rangle\rangle$ means averaging over

(23) Hurst, J. C.; Henderson, T. A.; Kreilick, R. W. *J. Am. Chem. Soc.* **1985**, *107*, 7294−7299.
(24) Iwasaki, M.; Toriyama, K. In *Electronic Magnetic Resonance of the Solid State*; Weil, J. A., Bowman, M. K., Morton, J. R., Preston, K. F., Eds.; Canadian Society of Chemistry: Ottawa, ON, Canada, 1987; p 545.
(25) Carrington, A.; McLachlan, A. D. *Introduction to Magnetic Resonance with Applications to Chemistry and Chemical Physics*; Harper and Row: New York, 1967; Chapter 7.
(26) Raitsimring, A.; Borbat, P.; Shokhireva, T.; Walker, F. A. *J. Phys. Chem.* **1996**, *100*, 5235−5244.

orientation and resonant fields which are also distributed in accord with individual line shape. Equation 8 was straightforwardly used for the simulations that follow.

The simulations were accomplished in the following manner: the averaging of eq 8 was performed numerically. For averaging over space we used a uniform grid for cos θ and ϕ of 1000 × 500 points. The orientation was accepted if $|(h\nu_0 - g_e{*}\beta{*}B_m)| \leq (g_e{*}\beta{*}B_1)/2$, where B_1 is the pulse amplitude and g_e is defined by eq 3. The individual line shape was evaluated from simulation of the EPR spectrum as a Gaussian, $\exp\{-((B - B_m)/\delta)^2\}$. The averaging over B was performed within the limits of $\pm 2\delta$ with step of 0.1δ. The time step and time interval in the simulations were chosen to be the same as in the corresponding experiments. The time domain pattern calculated in this way was then subjected to the same FT procedure that was used in the experiment with the experimental value for the dead time.

As one can see from eqs 5−8, the amplitude and position of lines in an ESEEM spectrum depend on the nuclear Larmor frequency and upon the isotropic and anisotropic hyperfine interactions. For disordered systems without g anisotropy these dependencies are well understood and have been described by Reijerse and Dikanov[27] and Dikanov *et al.*[28] Their analysis is qualitatively applicable for partially oriented systems; therefore, before presenting the results of the numerical simulations, we briefly review the behavior of a line in the vicinity of the double nuclear frequency, $2\nu_I$, by assuming that the characteristic value of the anisotropic interaction $|g\ T| < |a|$ or ν_I.

For the case of $\nu_I \gg a/2$ the line at $2\nu_I$ is the combinational $I(\nu_+)$. The position of this line is shifted from $2\nu_I$ to *higher* frequencies. The amplitude of this line (and all others as well) is proportional to $(gT/\nu_I)^2$; i.e., it decreases with increasing operational frequency as $(\nu_0)^{-2}$. Under these conditions the estimated absolute intensity of the $I(\nu_+)$ line for a Mo(V)···P distance of 3.2 Å and a resonant field of 3500 G is ≤0.7%.

For the opposite situation, $\nu_I \ll a/2$, the line at $2\nu_I$ is the combinational $I(\nu_-)$ line. The position of this line is shifted from $2\nu_I$ to *lower* frequency. The amplitude of this line is proportional to $(\nu_I/a)^2(T/a)^2$ and increases with increasing operational frequency. The absolute intensity evaluated using the same parameters given above and $a = 20$ MHz should not exceed 0.2%.

More complicated behavior is observed at the so-called "cancellation" condition, i.e., in the case when the hyperfine field on the nucleon matches the external field. In such a situation all three lines $I(\nu_{\alpha,\pm})$ are merged to form a composite line in the vicinity of $2\nu_I$, and the intensities of $I(\nu_\alpha)$ and $I(\nu_\pm)$ may be as high as 50 and 25%, irrespective of the magnitudes of $|a|$ and $|gT|$. Furthermore, a composite line may show any relative sign and any sign of Δ in the vicinity of $0 < (2\nu_I - |a|)/|gT| < 1$.

As noted above and shown in Figure 5, the experimental results show that the intensity of the line at $2\nu_p$ passes through a maximum as ν_0 is increased through 10−12.7 GHz. In accord with qualitative analysis, this result could be interpreted to mean that the system reaches the cancellation condition at $2\nu_p$ of 13−16 MHz. As just explained, the observation of a cancellation condition requires that the line should consequently transit from $I(\nu_-)$ to $I(\nu_+)$, passing through a composite line that is a mixture of $I(\nu_{\alpha,\pm})$, as ν_0 increases. Several other experimental observations are consistent with the interpretation just discussed. For example, starting from $\nu_0 \geq 11$ GHz, we may assume that the observed line is $I(\nu_+)$, because it has positive shift (Δ) and negative sign. The observed line at $\nu_0 = 10$ GHz would then be $I(\nu_{\alpha,-})$ because the sign of Δ is negative (at least at some field positions; see Figure 6). This assignment of line types is implicitly confirmed by the absence of a stimulated echo for the P-related line. As is well-known,[22] in stimulated echo only lines at the fundamental frequencies can be observed, with half the amplitude of those in a primary echo. Therefore, at $\nu_0 \geq 11$ GHz we would not expect to see lines in stimulated echo. At $\nu_0 < 11$ GHz the fundamental part of the composite line, as estimated from the $I(\nu_+)$ obtained in the two-pulse experiments, is not expected to exceed the noise level. Thus, based on the discussion just given, it would be tempting to assume that we have observed a cancellation condition and immediately evaluate the magnitude of the isotropic and anisotropic interactions.

However, such a simple assumption does not work because the maximum magnitude of the modulation amplitude that is experimentally observed (2%) differs by more than 1 order of magnitude from what one would expect from theory at the cancellation condition (∼50%). By all accounts this difference is too big to be explained by partial excitation (which we already took into account), additional nuclear relaxation, and other such factors that are usually invoked in ESEEM when experimental and calculated modulation amplitudes do not match each other.

We next considered the fact that the Mo(V) center may be ligated by more than one phosphate group, as proposed by George *et al.*[17] Each of these might have different isotropic (and anisotropic) constants and show different types of lines ($I(\nu_\alpha)$ or $I(\nu_\pm)$) at $2\nu_P$, depending on ν_0, with appropriate sets of parameters. However, allowing for multiple phosphates still fails to explain the intensity behavior, because to explain all the experimental observations the interaction with at least one of the nucleons has to pass through a cancellation condition with ν_0 and has to show a singularity in the amplitude of modulation.

An alternative explanation, which would reasonably account for all of the experimental data, may be provided by the assumption that a distribution of hyperfine parameters for the Mo···P interaction contributes to the observed traces. Indeed, to satisfy the experimental data one has only to assume that this distribution is wide enough to overlap the experimental range of $2\nu_P$, $0 < a < 19.5$ MHz. In such a situation, the proportion of the molecules in which parameters of Mo···P HFI are close to the cancellation condition will give the major contribution to the modulation intensity. As we already mentioned, the maximal amplitude of modulation in the cancellation condition is 50% for fundamental frequencies and 25% for combinational ones, and the interval of frequencies where cancellation occurs is on the order of magnitude of the anisotropic interaction, gT. So, for instance, if T is 0.5 MHz and the a's are uniformly distributed over the interval 0−20 MHz, then one would expect that the maximal intensity $I^*(\nu_m)$ would not exceed 1.25−2.5; also, the intensity should depend only slightly on ν_0, and the line would be positioned near $2\nu_P$. At this level of explanation, it is hard to predict which type of lines will predominate in the spectra. For this reason we performed the simulation of spectra for some model situations. For simulation we used eq 8 with additional averaging over the a distribution. For simplicity in particular simulations we assumed that the axes of the tensor of the anisotropic interaction $\mathbf{D}'$ coincided with the axes of the $\mathbf{g}$ tensor, $\mathbf{D}' = (T,T,-2T)$, and that the a distribution was uniform. As in our experiments, the simulations were performed at a given ν_0, stepping through the EPR spectrum with a stepsize of 5−6 G. In this way a set of lines $I(\nu)$ was obtained, each one corresponding to a particular

(27) Reijerse, E. J.; Dikanov, S. A. *J. Chem. Phys.* **1991**, *95*, 836−845.
(28) Dikanov, S. A.; Spoyalov, A. P.; Hüttermann, J. *J. Chem. Phys.* **1994**, *100*, 7973−7983.

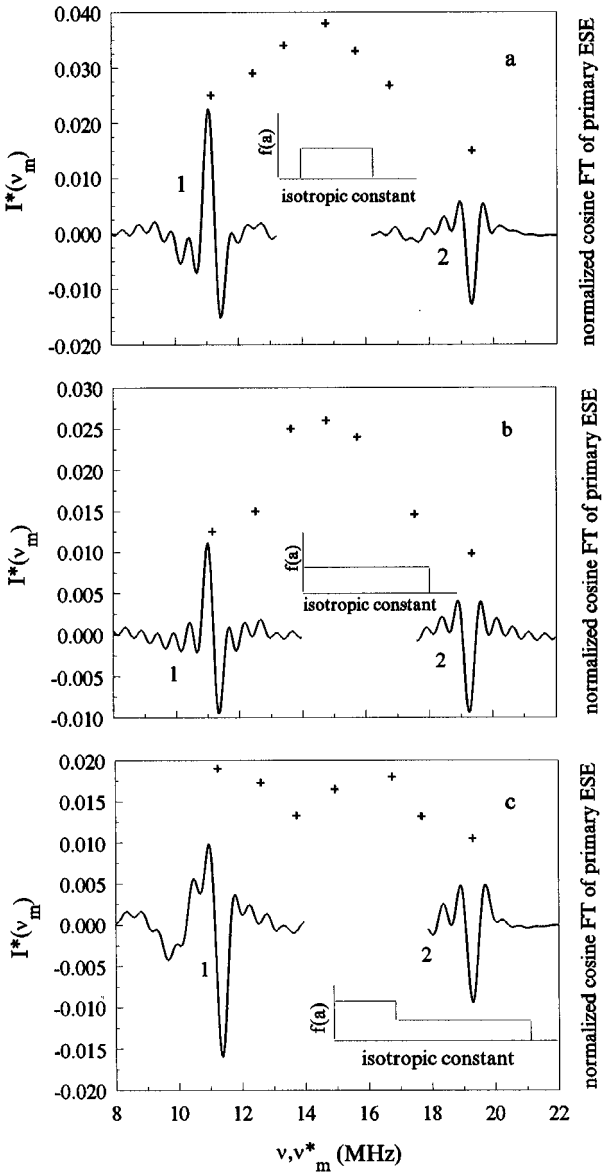

Figure 7. Crosses: Dependence of $I^*(\nu_m)$ on ν^*_m, obtained for simulated spectra, for various distributions $f(a)$ of the isotropic constant a. Curves: the simulated $I(\nu)$ at the magnetic fields corresponding to $I^*(\nu_m)$ at $\nu_0 = 8.904$ GHz (1) and $\nu_0 = 15.281$ GHz (2). Insets: schematic representations of the appropriate isotropic constant distribution function $f(a)$. The upper limit of a for all cases is 15 MHz; the lower limit of a for (a) and the position of the step for (c) is 5 MHz. The axes of the **D′** and **g** tensors in all the calculations are chosen to be coincident. For (a) and (b) $T = 0.5$ MHz; for (c) $T = 0.4$ MHz (see eq 3).

field (cf. Figure 4). From the set of maximum amplitudes of these lines, $I(\nu_m)$, the maximal one, $I^*(\nu_m)$ was taken and plotted vs ν^*_m. The simulations were repeated at a set of ν_0 values, thus generating a synthetic parametric curve comparable to that seen in Figure 5. The range of ν_0's and step over ν_0 in the simulation were approximately the same as in the experiment. The simulated plot of $I^*(\nu_m)$ vs ν^*_m for $T = 0.5$ MHz and a uniformly distributed over the ranges 5−15 and 0−15 MHz is shown in Figure 7, which also depicts entire line shapes, $I(\nu)$, for given $I^*(\nu_m)$'s at low and high ν_0. Figure 7 shows that $I(\nu)$ is a composite line, a mixture of $I(\nu_\alpha)$ and $I(\nu_+)$, for both distributions at low ν_0. As ν_0 increases, the $I(\nu)$ becomes solely an $I(\nu_+)$ line. The transition from a composite line to an $I(\nu_+)$ line depends upon the width of the a distribution and occurs at $\nu_0 > 12.7$ GHz for the first case and at $\nu_0 > 11$ GHz for the second one. The maximal intensities $I^*(\nu_m)$ vary with ν_0 in both cases by a factor of 2.5−3. The absolute value of the $I^*(\nu_m)$ does not exceed 3.8% for the first case and 2.6% for the second one. Therefore, as we evaluated above, the maximal modulation amplitude is proportional to the ratio of gT and the width of the a distribution. Furthermore, the spectrum consists of only one line near $2\nu_p$, which is either a composite one or a combinational one, and the amplitude of this line does not vary substantially with ν_0. All of the above show that the simulation closely approximates the experimentally observed dependence of the $I^*(\nu_m)$ on ν^*_m throughout the range of ν_0, although for the first type of a distribution the amplitudes are still higher than in the experiment, and for both of them the transition from a composite line to $I(\nu_+)$ occurred at higher ν_0. Because too many parameters are involved (the shape of the distribution, mutual orientation of the **g** and **D′** tensors, the parameters of anisotropic interaction), their quantitative determination is far beyond any reasonable speculation given the limitations on the information provided by the experiments. However, we can state that to more closely approximate the experimental dependence of $I^*(\nu_m)$ on ν^*_m, one has to either decrease the anisotropic interaction or increase the width of a in the simulation. The latter option is unlikely because the line width in the CW-EPR spectrum for samples prepared in D_2O buffer was ∼8.5 MHz. This line width is caused by Mo(V) interaction with all magnetic nuclei (D, H, P), and the interaction with P (on average) cannot exceed this value. In terms of a uniform a distribution, this imposes the restriction $a < 17$ MHz. Also, increasing the width of the distribution shifts the range of ν_0 where the transition from a composite to a combinational line occurs to higher ν_0 values. So, most probably the a distribution is shifted to low frequencies. Following this reasoning we performed one more simulation, slightly decreasing T to 0.4 MHz and using a more complicated distribution function as shown in the inset of Figure 7c. This set of parameters resulted in a decrease of $I^*(\nu_m)$ to the experimental range of magnitudes, Figure 7. The range of ν_0 where the change of line type occurs for this simulated set also corresponds to the experimental one. All this discussion allows us to conclude that most probably the magnitude of T is 0.4−0.5 MHz and the a distribution function is close to that shown in Figure 7b,c. In the PD approximation this value of T corresponds to a Mo···P distance of 3.2−3.3 Å. For a monodentate phosphate ligand this gives a Mo−O bond length of ∼2.25 Å; which although somewhat long, is within the known range for Mo−phosphate complexes.[29]

Conclusions

These first multifrequency ESEEM studies of the Mo(V) center of SO in phosphate buffer provide direct proof that the Mo is ligated by at least one phosphate group and demonstrate the power of this technique for detecting weakly coupled nuclei. We believe that the coordinated phosphate group(s) does (do) not adopt a fixed orientation, and as a result, a description of the Mo···P hyperfine interaction requires the introduction of a distribution of such orientations (structure **2**). Recently, the idea

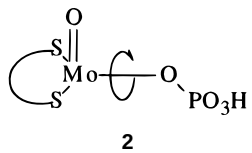

2

of a distribution for nonrigid organic molecules was independently exploited by Wamcke and McCracken to explain

(29) See for example: Fischer, J.; Ricard, L.; Toledano, P. *J. Chem. Soc., Dalton Trans.* **1974**, 941−946.

observations in an unrelated investigation.[30] In that case, the distribution hypothesis provided the only explanation for their observed results. We are currently pursuing further quantum chemical calculations on model systems in order to better understand how the position of ligation (axial or equatorial) and a range of phosphate group orientations may cause such a distribution of hyperfine coupling.

Combining our ESEEM results on SO in phosphate buffer with other spectroscopic and chemical data on the enzyme provides important insights concerning the structural proposals for the various forms of SO shown in Scheme 1. Prior EXAFS investigations of SO indicate one terminal oxo ligand when Mo is in the +4 or +5 oxidation state.[16,31] In addition, phosphate analysis of SO (in non-phosphate buffer) by Johnson *et al.*,[32] and mass spectral data obtained in our laboratories,[19] indicate only one pterin ligand per Mo for this enzyme (cf. structure **1**). The two sulfur atoms from this ligand account for two more coordination sites. Thus, the nature of four of the Mo coordination sites can be specified with confidence (one oxo, two sulfurs, and one phosphate or OH). In addition, recent genetic studies have shown that one of the cysteine residues in rat liver SO is essential for catalytic activity, and it was also concluded to be a ligand to molybdenum.[33] This cysteine is conserved in all SO's and the related nitrate reductases[33] and probably plays the same catalytic role in each case.

The catalytic cycle of SO was previously investigated by both steady-state[34] and rapid-reaction[19,35] kinetic techniques, and these investigations showed that anions such as phosphate and sulfate are inhibitors of the enzyme. On the basis of their CW-EPR studies, Bray and co-workers previously suggested that direct coordination of anion to the Mo center could be responsible for such inhibition.[10−13] Our positive identification of a Mo−phosphate adduct provides strong support for this hypothesis, as shown in Scheme 2. Initially, the reduced form of SO is generated by direct oxo atom transfer to sulfite, as proposed by Brody and Hille.[35] We suggest that, in the catalytic cycle, water displaces sulfate as a necessary step in the regeneration of the starting Mo(VI) species. In the presence of high phosphate concentrations, the phosphate-inhibited form is then formed either by direct displacement of the sulfate or by funneling off the hydroxo species. Note that, in addition, phosphate at low pH could also inhibit the enzyme by disruption of the essential Mo−cysteine bond. We are presently completing ENDOR and ESEEM investigations of SO in high- and low-pH buffers, in which we are studying weak hyperfine interactions of the unpaired electron of the Mo atom with nearby N and nonexchangeable H atoms. These studies are providing additional valuable information about the Mo(V) coordination environment of reduced SO that will be the subject of future communications.

Scheme 2

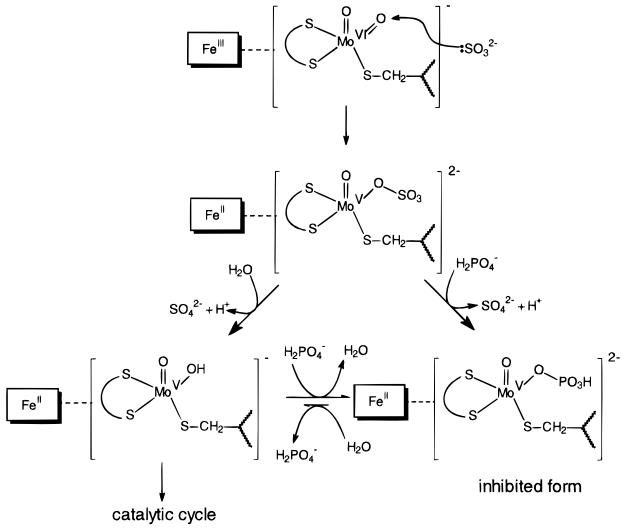

Acknowledgment. We thank Professor R. Hille for providing a preprint of ref 5 prior to publication, F. A. Walker and N. Shokhirev for helpful discussions, and W. A. Wehbi for assistance in the enzyme purification. Financial support received from the National Institute of Health (Grant GM 37773), the National Science Foundation (Grants DIR 9016385 and BIR 9224431 for the EPR spectrometer), and the Materials Characterization Program of the University of Arizona are gratefully acknowledged. Finally, we appreciate several helpful comments from the reviewers.

IC9607806

(30) Wamcke, K.; McCracken, J. *J. Chem. Phys.* **1995**, *103*, 6829−6840.
(31) Cramer, S. P.; Wahl, R.; Rajagopalan, K. V. *J. Am. Chem. Soc.* **1981**, *103*, 7721−7727.
(32) Johnson, J. L.; Hainline, B. E.; Rajagopalan, K. V.; Arison, B. H. *J. Biol. Chem.* **1984**, *259*, 5414−5422.
(33) Garrett, R. M.; Rajagopalan, K. V. *J. Biol. Chem.* **1996**, *271*, 7387−7391.
(34) Kessler, D. L.; Rajagopalan, K. V. *Biochim. Biophys. Acta* **1974**, *370*, 389−398.
(35) Brody, M. S.; Hille, R. *Biochim. Biophys. Acta* **1995**, *1253*, 133−135.